Elasto-dynamic analysis of a gear pump. Part III: experimental validation procedure and model extension to helical gears

E. Mucchi (*), G. Dalpiaz (*)

(*) Engineering Department, University of Ferrara
Via Saragat, 1 I-44122 Ferrara, Italy.

Corresponding Author:
Emiliano Mucchi
Engineering Department, University of Ferrara
Via Saragat, 1 I-44122 Ferrara. Italy
email: **emiliano.mucchi@unife.it**
tel: +39 0532 974913
fax: +39 0532 974870

ABSTRACT

This work concerns external gear pumps for automotive applications, which operate at high speed and low pressure. In previous works of the authors (Part I and II, [1][2]), a non-linear lumped-parameter kineto-elastodynamic model for the prediction of the dynamic behaviour of external gear pumps was presented. It takes into account the most important phenomena involved in the operation of this kind of machine. Two main sources of noise and vibration can be considered: pressure period variation and gear meshing. The model has been used in order to foresee the influence of working conditions and design modification on vibration generation. The model's experimental validation is a difficult task. Thus, Part III proposes a novel methodology for the validation carried out by the comparison of simulations and experimental results concerning forces and moments: it deals with the external and inertia components acting on the gears, estimated by the model, and the reactions and inertia components on the pump casing and the test plate, obtained by measurements. The validation is carried out comparing the level of the time synchronous average in the time domain and the waterfall maps in the frequency domain, with particular attention to identify system resonances. The validation results are globally satisfactory, but discrepancies are still present. Moreover, the assessed model has been properly modified for the application to a new virtual pump prototype with helical gears in order to foresee gear accelerations and dynamic forces. Part IV is focused on improvements in modelling and analysis of the phenomena bound to the pressure distribution around the gears in order to achieve results closer to measured values. As a matter of fact, the simulation results have shown that the variable meshing stiffness has a notable contribution on the dynamic behaviour

of the pump but this is not as important as the pressure phenomena. As a consequence, the original model was modified with the aim at improving the calculation of pressure forces and torques. The improved pressure formulation includes several phenomena not considered in the previous one, such as the pressure variations at input and output ports, as well as an accurate description of the trapped volume and its connections with high and low pressure chambers. The importance of these improvements are highlighted by comparison with experimental results, showing satisfactory matching.

KEYWORDS: External gear pumps; experimental validation; casing and gear acceleration; dynamic analysis; elastodynamic behaviour.

NOMENCLATURE

Latin symbols

a	Centre distance of gear pair.
b	Face width of both gears.
B	Relief groove dimension.
C_j	Viscous damping coefficient of tooth pair j.
C_T	Torsional viscous damping coefficient of the driving shaft.
E_j	Profile error of tooth pair j.
f_{bxk}	Bearing reaction applied to gear k in direction X.
f_{byk}	Bearing reaction applied to gear k in direction Y.
f_{mg}	Meshing force.
f_{mgj}	Meshing force of tooth pair j.
f_{mgm}	Mean meshing force over one pitch.
f_{pxk}	Pressure force applied to gear k in direction X.
f_{pyk}	Pressure force applied to gear k in direction Y.
F_P	High-pressure pipe force.
g	Backlash along the line of action.
J_G	Moment of inertia of pump and plate with respect to the center of mass.
J_k	Moment of inertia of gear k.
K_j	Stiffness of tooth pair j in case of spur gears.
K_T	Torsional stiffness of the driving shaft.
m_k	Mass of gear k.
M_m	Motor driving torque.
M_{pk}	Pressure torque applied to gear k.
m_{pp}	Mass of pump and plate.
r_{bk}	Base radius of gear k.
R_{pk}	Radius of the pitch circle of gear k.
$R_{X'12}$	Sum of the force sensor reactions in X'_1 direction concerning sensors 1 and 2
$R_{X'34}$	Sum of the force sensor reactions in X'_1 direction concerning sensors 3 and 4
$R_{Y'23}$	Sum of the force sensor reactions in Y'_1 direction concerning sensors 2 and 3
$R_{Y'14}$	Sum of the force sensor reactions in Y'_1 direction concerning sensors 1 and 4
t	Periodic time ($0 \le t < T$).
T	Meshing period.

$\ddot{x}'_C, \ddot{x}'_D$ C and D accelerometer accelerations in direction X'_1.

x_k, y_k Coordinates of the centre of gear *k* in reference frame $O_kX_kY_k$.

x^*_k, y^*_k Coordinates of the centre of gear *k* in the SEP.

x'_G, y'_G Center of mass of pump and plate in reference frame $O'_1X'_1Y'_1$.

$\ddot{x}'_{O_1}, \ddot{y}'_{O_1}$ Plate acceleration in point O_1 in direction X'_1 and Y'_1.

$\ddot{y}'_A, \ddot{y}'_B$ A and B accelerometer accelerations in direction Y'_1.

Greek symbols

α_w Pressure angle in working condition.

β Helix angle on the pitch circle.

$\tilde{\varepsilon}$ Contact ratio.

γ_m Proportionality constant between viscous damping coefficient and stiffness of a tooth pair.

γ_T Proportionality constant between viscous damping coefficient and stiffness of the driving shaft.

θ Angular coordinate.

θ' Angular displacement of force plate and pump casing in reference frame $O'_1X'_1Y'_1$.

θ_k Angular displacement of gear *k* in reference frame $O_kX_kY_k$.

θ_0 Angular displacement of the electrical drive in reference frame $O_kX_kY_k$.

Subscripts

j=a, b, c, d Denotes pairs of teeth.

k=1, 2 Denotes gears.

L Stands for linearized.

1. INTRODUCTION

Noise Vibration and Harshness (NVH) is one of the most important topics in the automotive industry [3]. Acoustic and vibration comfort is another of the key features in a new design and consequently suppliers of automotive components need to satisfy more restrictive requirements defined by final manufacturers. Moreover, in order to achieve the goals defined by the final customer, the component suppliers need to increment the resources on design and testing tasks. This scenario increases the interest on modelling the dynamic behaviour of mechanical systems as a way to improve the initial design reducing testing efforts. A good dynamic model could be a useful and powerful tool for the identification of noise and vibration sources and for design improvements. Models should be simple but at the same time should provide a prediction of the dynamic behaviour in a sufficiently accurate and reliable fashion. The development of this kind of tool requires a good analysis of the system in order to define the most important phenomena that must be included in the model as well as the formulation or modification of theories that allow the description of each system element.

In this work a numerical model of the vibratory behaviour of an external gear pump for automotive application is presented. Part I and II ([1][2]) describe in detail the non-linear lumped-parameter kineto-elastodynamic model. Part III is devoted to the experimental validation and to the model extension to helical gears; Part IV presents the pressure formulation improvements.

The pump being studied operates at high speed and low pressure. In principle, two main sources of noise exist in this kind of machinery: fluid borne-noise as a consequence of the flow from the low to the high pressure chambers and structural borne-noise due to gear meshing. When the pressure is higher, the fluid borne-noise becomes dominant. Nevertheless, on the basis of experimental results regarding this type of gear pump, the emitted noise includes not only fluid borne-noise, but it has important components due to mechanical vibrations. Moreover, the fluid–structure interaction between the oil and pump casing may play a role in producing noise. Considering the complex nature and the combination of both excitation sources, design is a difficult task requiring a great number of experimental tests. This fact increases the interest in developing a model that includes pressure and gear meshing phenomena simultaneously with the aim at predicting the effects of design modifications reducing the number of tests required for prototype development and design improvement. In the literature, works that only deal with the dynamic behaviour of gear pairs for design and NVH reduction [4][5] [6][7][8], as well as the pressure evolution in a tooth space during the pump rotation [9][10][11] and the oil bearing behaviour[12][13][14] were found, but such effects have been shown and discussed separately. Other authors [11][15] have thoroughly investigated gear pumps, precisely determining the eccentric position assumed by the gears inside the pump casing as a function of operational conditions. However, apart from authors' papers, works that take into account all the above dynamic effect in order to evaluate the dynamic behaviour of the gear pump in terms of gear acceleration cannot be found in the literature.

In this context, a non-linear lumped-parameter kineto-elastodynamic model for the prediction of the dynamic behaviour of external gear pumps has been developed and presented in Part I [1] and Part II [2]. The model has six degrees of freedom and includes the main important phenomena involved in the pump operation as time-varying oil pressure distribution on gears, time-varying meshing stiffness and hydrodynamic journal bearing reactions. Casing wear, backlash between the meshing teeth and profile errors are considered as well, improving the model features. It is worth noting that all these important effects are included in the same model in order to take their interactions into account. In this way the resulting model is a useful tool for studying the effects of design parameters concerning both gears (profile shape and errors) and geometry of other components (relief grooves milled in the bearing blocks, clearances between

moving components, casing internal profile shape, etc) and of operational parameters as oil viscosity, operational pressure and rotational speed. It is a first step in the perspective of developing a combined model for the simulation of casing vibrations as well as noise propagation, since this model can estimate gear vibrations as well as the variable forces exciting the external casing. As a matter of fact, the combination of these excitation forces with the structural frequency response functions of the pump casing produces the operational accelerations of the casing, which in turn are inputs for a further acoustical analysis. However, the reduction of gear vibrations and excitation forces applied to the casing determines the reduction of pump noise and vibration.

A good model should be a good representation of the real machine and therefore should have a good correspondence with experimental measurements. In this respect, the proposed model must be validated using experiments in order to verify its usefulness, limitations and possible improvements. This task is not very easy for complex systems such as external gear pumps because it is not easy to directly obtain vibration data concerning rotating components. During the validation phase, model parameters can be modified in order to better approach the real experimental behaviour. This could be also a critical task because good experiments are as rare as good theories and complex systems sometimes introduce additional difficulties associated with the availability of directly comparing measurement data with model outputs. In the literature, several researchers [10][11][16] [17] have measured the time variation of the tooth space pressure in an external gear pump by using a pressure transducer fitted in the gears. The pressure signal from the miniature sensor mounted in the bottom of a tooth space is taken out via slip-rings for acquisition and further analysis obtaining the so-called pressure distribution around the gears, i.e. the pressure value in a tooth space during a complete rotation of the gears. However, we are interested in the validation of the whole “dynamic model”, i.e. the model that allows the gear accelerations to be estimated and not only the pressure model, the meshing and the journal bearing models. Moreover, the experimental measurements carried out in [16][10][11] were performed on medium-size external gear pumps where the tooth space dimension could house a pressure transducer. In our case, the pump being studied (called GENB) is a small-size external gear pump and the inter-tooth space is narrow. For these reasons, an original validation procedure has been developed “ad hoc” for the GENB pump in order to verify the dynamic model. Briefly, model validation is based on the comparison between simulations and experimental results concerning dynamic forces and moments: it deals with the external and inertia components acting on gears, estimated by the model, and the reactions and inertia components acting on the pump casing and on the test plate, obtained by experimental tests. These are the components that can excite casing vibrations and produce noise; consequently, their estimation has a practical interest for noise reduction. The validation is carried out comparing the Root Mean Square (RMS) level of the time

synchronous average of vibration time data and relative waterfall maps in the frequency domain, with particular attention to identify system resonances.

The third part of this work (Part III) mainly presents the original validation procedure and results. In particular in Section 2 the mechanical system as well as the developed original model [1][2] are briefly described highlighting the main features. As stated above, the model is highly non-linear and the natural frequencies cannot be defined. For validation purpose it is useful to evaluate the natural frequencies and mode shapes of the correspondent undamped linearized model, in order to compare these natural frequencies with the experimental resonances. In this context, Section 3 presents the model linearization and the relative results in terms of natural frequencies and mode shapes. Section 4 addresses the experimental test set up with particular reference to the experimental instrumentation used and the validation procedure. The comparison between experimental and simulation quantities is carried out both in the time and in the frequency domain and the results are given in Section 5. Once the model has been experimentally assessed, it can be used in order to predict the effects of design modifications, so reducing the number of tests required for design improvement. Indeed, in Section 6 the original model was properly modified in order to evaluate gear accelerations and dynamic forces of a new virtual pump prototype, namely GENB_P, before the physical prototype is available. The comparison of the dynamic behaviour of the new pump and the GENB pump is also shown in terms of pressure forces and gear accelerations. Eventually, Section 7 is devoted to concluding remarks.

2. EXTERNAL GEAR PUMP DESIGN AND MODEL FORMULATION

In this section, a short description of the main components and terminology related with external gear pumps is presented as well as an overview of the developed elastodynamic model. The complete model formulation and implementation can be found in previous works of the authors, Part I and II, [1][2]. The most usual configuration of the pump being studied has two twin gears, which are assembled by a couple of lateral floating bearing blocks packed inside a close tolerance casing, see Figure 1. Lateral floating bearing blocks act as a seal for the lateral ends but also as supports for gear shafts by means of two hydrodynamic bearings, which have a drainage circle milled in the internal face connected to the low pressure chamber. The operating principle of external gear pumps is simple: the fluid is carried around the outside of each gear from the intake to the discharge side (from left to the right in Figure 2(a)) within the space bounded between two subsequent gear teeth, the casing and the bearing blocks. As the gears turn, the pressure of these isolated spaces progressively increase up to the high pressure. In the gear meshing area, when two tooth pairs become into contact, a trapped volume could arise and could undergo a sudden volume reduction and consequently a

violent change in its pressure. To avoid this, the trapped volume is put in communication with the high or low pressure chambers. That is the role of the relief grooves milled in the internal face of lateral bearing blocks whose shape and location are so important in the resulting dynamic behaviour. Furthermore, bearing blocks should be also hydraulically balanced in axial direction with the aim of avoiding misalignments between gear shafts and journal bearings. To achieve that, a rubber seal located in the external face of the endplates is used. This seal defines two areas subjected to high or low pressure; such a pressure should balance the pressure exerted in the opposite face by the pressure in the isolated spaces and in the high pressure chamber. One of the gears (gear 1) has a long shaft that is connected by an Oldham coupling with an electrical motor allowing some misalignments between them. In this work the interest is focused on external gear pumps for automotive applications as in steering systems, which operate at high speed (from 1500 to 3400 rpm) and low pressure (from 3.5 to 100 bar).

The main important phenomena involved in the pump dynamic behaviour have been included in the numerical model: pressure distribution variation, meshing forces and hydrodynamic bearing reactions. A schematic of the model is shown in Figure 2(b). It is a planar model with six degrees of freedom (x_1, y_1, θ_1, x_2, y_2, θ_2). Two different reference frames for each gear are used (see Figure 2(a)), both having their origins coinciding with the centres of the gears. In reference frames $O_1X_1Y_1$ and $O_2X_2Y_2$, the X-axis and the Y-axis are perpendicular and parallel to the line of action, respectively. On the other hand, in reference frames $O_1X'_1Y'_1$ and $O_2X'_2Y'_2$, the Y'-axis is along the line connecting the centres of the gears and the X'-axis is orthogonal (Figure 2(a)). The model input is coordinate θ_0, representing the angular displacement of the electric drive, assumed to rotate at constant speed. Coordinate θ_0 is connected to gear 1 by a torsional spring-damper element being K_T the torsional shaft stiffness and C_T the proportional viscous damping. Meshing stiffness and damping, profile errors (obtained from metrological measurements) as well as lubricant squeeze are included in each one of the contact blocks in Figure 2(b) representing the *Direct (DLA) and Inverse (ILA) lines of action*. The gears are low contact ratio gears ($\tilde{\varepsilon}$ =1.35), so on each line of action there will be one or two meshing tooth pairs. To consider this condition, every one of the four possible pairs of teeth in contact is associated to a stiffness (K_j) and to a viscous damper of coefficient C_j, with j=*a, b, c, d.* This damper globally takes the structural damping as well as other damping effects into account. The damper coefficient is taken proportional to the corresponding stiffness if teeth are into contact; when the tooth separation occurs, the damper coefficient is computed in order to represent the lubricant squeeze effect. Quantities with subscripts *a* and *b* are related to the pairs of teeth along the DLA while subscripts *c* and *d* are related to the pairs of teeth along the ILA. Backlash *g* between the meshing teeth is also included, as well as the

possibility of tooth contact or separation on both contact lines. Meshing stiffness is obtained using Kuang's formulation [18] for spur gears including the Hertzian contact stiffness as a constant term for each angular position.

The pressure evolution around the gears is calculated taking advantage of a mathematical model grounded on the Euler's approach. The pressure model has been developed by identifying the "sealed" spaces between teeth, bearing blocks and casing as tooth space control volumes (see Figure 2a). Each control volume is treated as an open thermodynamic system with mass transfer with its surroundings. The application of the continuity equation and the state equation of the fluid, assuming an adiabatic and isentropic transformation to each control volume allows the pressure inside the tooth spaces to be evaluated [1][9]. The pressure evolution in the remaining parts of the gears (meshing zone, inlet and outlet chambers) is not calculated by using the above-mentioned control volume approach, but it is supposed known; in particular, the pressure in the inlet and outlet chamber is considered as constant and equal to the atmospheric pressure and the output pressure, respectively. Moreover, it is needed to model the phenomena occurring in the gear meshing area, when two tooth pairs come into contact. In this transition phase, for a time interval equal to 3.5/100 of the meshing period, the trapped volume is simultaneously put in communication with the inlet and outlet volumes due to the shape and dimension of the relief grooves. During this time interval a linear decrease of the pressure in the trapped volume from the outlet to the inlet value has been assumed. The latter assumption has an experimental origin: experimental measurements of the pressure evolution in a tooth space for a complete gear rotation performed in external gear pumps [16][19] depict an almost linear pressure transient in the meshing area. Pressure calculation includes also the casing inner profile modified by the running-in process that takes place at the end of the manufacturing phase in order to increase pump efficiency. The displacement toward the low pressure chamber of the lateral floating bearing blocks is taken into account too. Once the pressure value for each gear angular position is known, the resultant pressure forces (f_{pxk}, f_{pyk}) and torque (M_{pk}) on each gear can be obtained. The non-linear reactions of the hydrodynamic journal bearings (f_{bxk}, f_{byk}) are implemented using the formulation proposed by Childs et al. [20], called "*finite impedance formulation*". Briefly, it consists on taking into account and composing the results yielded from the "short bearing" and "long bearing" theories.

The explicit and complete formulation can be found in [1][2]. Hereafter, the equations of motion are reported in a particular case, very common in practice, where the meshing contact occurs only along the DLA and the lubricant squeeze effect is neglected. The equations of motion in $O_kX_kY_k$ reference frame (Figure 2(a)), have the following form (see the list of symbols in Nomenclature):

$$\begin{cases} m_1\,\ddot{x}_1 = f_{bx1}(x_1, y_1, \dot{x}_1, \dot{y}_1, \dot{\theta}_1) + f_{px1}(x_1, y_1, \theta_1, \dot{\theta}_1) \\ m_1\,\ddot{y}_1 = f_{by1}(x_1, y_1, \dot{x}_1, \dot{y}_1, \dot{\theta}_1) + f_{py1}(x_1, y_1, \theta_1, \dot{\theta}_1) + f_{mg}(y_1, y_2, \dot{y}_1, \dot{y}_2, \theta_1, \theta_2, \dot{\theta}_1, \dot{\theta}_2) \\ J_1\,\ddot{\theta}_1 = -r_{b1}\; f_{mg}(y_1, y_2, \dot{y}_1, \dot{y}_2, \theta_1, \theta_2, \dot{\theta}_1, \dot{\theta}_2) - M_{p1}(\theta_1) + M_m(\theta_0, \dot{\theta}_0, \theta_1, \dot{\theta}_1) \\ m_2\,\ddot{x}_2 = f_{bx2}(x_2, y_2, \dot{x}_2, \dot{y}_2, \dot{\theta}_2) + f_{px2}(x_2, y_2, \theta_2, \dot{\theta}_2) \\ m_2\,\ddot{y}_2 = f_{by2}(x_2, y_2, \dot{x}_2, \dot{y}_2, \dot{\theta}_2) + f_{py2}(x_2, y_2, \theta_2, \dot{\theta}_2) - f_{mg}(y_1, y_2, \dot{y}_1, \dot{y}_2, \theta_1, \theta_2, \dot{\theta}_1, \dot{\theta}_2) \\ J_2\,\ddot{\theta}_2 = r_{b2}\; f_{mg}(y_1, y_2, \dot{y}_1, \dot{y}_2, \theta_1, \theta_2, \dot{\theta}_1, \dot{\theta}_2) - M_{p2}(\theta_2) \end{cases} \tag{1-6}$$

where motor driving torque M_m is evaluated on the basis of the torsional stiffness-damping proprieties of the driving shaft as:

$$M_m(\theta_0, \dot{\theta}_0, \theta_1, \dot{\theta}_1) = K_T\left(\theta_0 - \theta_1\right) + C_T\left(\dot{\theta}_0 - \dot{\theta}_1\right) \tag{7}$$

and meshing forces f_{mg} along the DLA are defined as:

$$\begin{aligned} f_{mg} &= f_{mga} + f_{mgb} \\ f_{mga} &= \left(r_{b1}\theta_1 - r_{b2}\theta_2 - y_1 + y_2 + E_a - \frac{g}{2}\right)K_a + \left(r_{b1}\dot{\theta}_1 - r_{b2}\dot{\theta}_2 - \dot{y}_1 + \dot{y}_2 + \dot{E}_a\right)\gamma_m K_a \\ f_{mgb} &= \left(r_{b1}\theta_1 - r_{b2}\theta_2 - y_1 + y_2 + E_b - \frac{g}{2}\right)K_b + \left(r_{b1}\dot{\theta}_1 - r_{b2}\dot{\theta}_2 - \dot{y}_1 + \dot{y}_2 + \dot{E}_b\right)\gamma_m K_b \end{aligned} \tag{8-10}$$

Error functions E_a, E_b, E_c, E_d are the displacement excitations representing the relative gear errors of the meshing teeth. The non-linear differential equations of motion are numerically integrated by using software Simulink. With the aim of integration time reduction, the so-called ‘static’ equilibrium positions (SEP) of the gear shaft axes inside the journal bearings are estimated before the integration of the equations of motion. In steady-state operational conditions, the gear axes periodically move, due to the periodic variation of pressure and meshing forces. The gear centreline trajectory is an orbit around an eccentric position with respect to the case. This eccentric position is not the actual gear axis position, but it can be considered as a reference position during the periodic motion of the axes. This position is obtained in the model by the ‘static’ equilibrium of gears. It is the equilibrium obtained in ideal conditions where the periodic variation of forces is neglected and the latter are taken as a constant value, equal to their mean value. With more details, the SEP is obtained by an iterative procedure that finds this equilibrium position taking into account the average value of the pressure forces and torques over one gear pitch, the mean meshing forces and the bearing reactions.

3. MODEL LINEARIZATION

The model is nonlinear and in principle the natural frequencies could not be defined. However, it can be useful to evaluate the natural frequencies and mode shapes of the correspondent undamped linearized model, in order to compare them with the experimental resonances shown in the following (Section 5). The undamped natural frequencies and mode shapes were calculated by solving a generalized eigenvalue problem involving the mass and the stiffness matrices of the mechanical system. To do that, the equations of motion Eqs. (1) to (6) have to be manipulated. Firstly, the bearing forces were linearized in the SEP (x^*_k, y^*_k) by the expansion in a Taylor series limiting the attention to the first terms, as follows [21]:

$$f_{bxk}(x_k, y_k, \dot{x}_k, \dot{y}_k, \dot{\theta}_k) = f_{bxk}(x_k^*, y_k^*, 0, 0, \omega_k) + \left(\frac{\partial f_{bxk}}{\partial x_k}\right)\left(x_k - x_k^*\right) + \left(\frac{\partial f_{bxk}}{\partial y_k}\right)\left(y_k - y^*_k\right) + \left(\frac{\partial f_{bxk}}{\partial \dot{x}_k}\right)\dot{x}_k + \left(\frac{\partial f_{bxk}}{\partial \dot{y}_k}\right)\dot{y}_k \tag{11}$$

$$f_{byk}(x_k, y_k, \dot{x}_k, \dot{y}_k, \dot{\theta}_k) = f_{byk}(x_k^*, y_k^*, 0, 0, \omega_k) + \left(\frac{\partial f_{byk}}{\partial x_k}\right)\left(x_k - x_k^*\right) + \left(\frac{\partial f_{byk}}{\partial y_k}\right)\left(y_k - y^*_k\right) + \left(\frac{\partial f_{byk}}{\partial \dot{x}_k}\right)\dot{x}_k + \left(\frac{\partial f_{byk}}{\partial \dot{y}_k}\right)\dot{y}_k \tag{12}$$

The partial derivatives in Eqs. (11) and (12) are calculated in the SEP (x^*_k, y^*_k) and called “bearing stiffness coefficients”

$$K^k_{xx} = -\frac{\partial f_{bxk}}{\partial x_k}; \quad K^k_{xy} = -\frac{\partial f_{bxk}}{\partial y_k}; \quad K^k_{yx} = -\frac{\partial f_{byk}}{\partial x_k}; \quad K^k_{yy} = -\frac{\partial f_{byk}}{\partial y_k} \tag{13}$$

and “bearing damper coefficients”

$$C^k_{xx} = -\frac{\partial f_{bxk}}{\partial \dot{x}_k}; \; C^k_{xy} = -\frac{\partial f_{bxk}}{\partial \dot{y}_k}; \; C^k_{yx} = -\frac{\partial f_{byk}}{\partial \dot{x}_k}; \; C^k_{yy} = -\frac{\partial f_{byk}}{\partial \dot{y}_k} \tag{14}$$

Thus, the nonlinear bearing reactions can be approximated as linear springs and damper elements. In order to yield the linearized meshing forces, further approximations were taken. Firstly, the variable meshing stiffness of tooth pair *a* and *b* were replaced by its mean value K_{avg} over the meshing period *T*:

$$K_{avg} = \frac{1}{T}\int_0^T \left[K_a(t) + K_b(t)\right]dt\,. \tag{15}$$

Secondly, backlash g between the meshing teeth, the error functions, the squeeze effect and the possibility of separation of the meshing teeth were neglected, leading to obtain the following linear system of equations of motion (the subscript L stands for "linearized"):

$$[M]\{\ddot{q}\}+[C]_L\{\dot{q}\}+[K]_L\{q\}=\{f^*_b\}+\{f_p\}+\{f_s\}+\{f_{ext}\} \tag{16}$$

where:

$$[M]=\begin{bmatrix} m_1 & 0 & 0 & 0 & 0 & 0 \\ 0 & m_1 & 0 & 0 & 0 & 0 \\ 0 & 0 & J_1 & 0 & 0 & 0 \\ 0 & 0 & 0 & m_2 & 0 & 0 \\ 0 & 0 & 0 & 0 & m_2 & 0 \\ 0 & 0 & 0 & 0 & 0 & J_2 \end{bmatrix} \tag{17}$$

$$[K]_L=\begin{bmatrix} K^1_{xx} & K^1_{xy} & 0 & 0 & 0 & 0 \\ K^1_{yx} & K^1_{yy}+K_{avg} & -r_{b1}K_{avg} & 0 & -K_{avg} & r_{b2}K_{avg} \\ 0 & -r_{b1}K_{avg} & K_T+r^2_{b1}K_{avg} & 0 & r_{b1}K_{avg} & -r_{b1}r_{b2}K_{avg} \\ 0 & 0 & 0 & K^2_{xx} & K^2_{xy} & 0 \\ 0 & -K_{avg} & r_{b1}K_{avg} & K^2_{yx} & K^2_{yy}+K_{avg} & -r_{b2}K_{avg} \\ 0 & r_{b2}K_{avg} & -r_{b1}r_{b2}K_{avg} & 0 & -r_{b2}K_{avg} & r^2_{b2}K_{avg} \end{bmatrix} \tag{18}$$

$$[C]_L=\begin{bmatrix} C^1_{xx} & C^1_{xy} & 0 & 0 & 0 & 0 \\ C^1_{yx} & C^1_{yy}+\gamma_m K_{avg} & -r_{b1}\gamma_m K_{avg} & 0 & -\gamma_m K_{avg} & r_{b2}\gamma_m K_{avg} \\ 0 & -r_{b1}\gamma_m K_{avg} & \gamma_T K_T+\gamma_m r^2_{b1}K_{avg} & 0 & r_{b1}\gamma_m K_{avg} & -r_{b1}r_{b2}\gamma_m K_{avg} \\ 0 & 0 & 0 & C^2_{xx} & C^2_{xy} & 0 \\ 0 & -\gamma_m K_{avg} & r_{b1}\gamma_m K_{avg} & C^2_{yx} & C^2_{yy}+\gamma_m K_{avg} & -r_{b2}\gamma_m K_{avg} \\ 0 & r_{b2}\gamma_m K_{avg} & -r_{b1}r_{b2}\gamma_m K_{avg} & 0 & -r_{b2}\gamma_m K_{avg} & r^2_{b2}\gamma_m K_{avg} \end{bmatrix} \tag{19}$$

$$\{q\}^t=\{x_1 \quad y_1 \quad \theta_1 \quad x_2 \quad y_2 \quad \theta_2\}$$

$$\{f^*_b\}^t=\{f^*_{bx1}+K^1_{xx}x^*_1+K^1_{xy}y^*_1 \quad f^*_{by1}+K^1_{yx}x^*_1+K^1_{yy}y^*_1 \quad 0 \quad f^*_{bx2}+K^2_{xx}x^*_2+K^2_{xy}y^*_2 \quad f^*_{by2}+K^2_{yx}x^*_2+K^2_{yy}y^*_2 \quad 0\}$$

$$\{f_p\}^t=\{f_{px1} \quad f_{py1} \quad -M_{p1} \quad f_{px2} \quad f_{py2} \quad -M_{p2}\}$$

$$\{f_s\}^t=\{0 \quad 0 \quad C_T\dot{\theta}_0+K_T\theta_0 \quad 0 \quad 0 \quad 0\}$$

$$f^*_{bxk}=f_{bxk}(x^*_k,y^*_k,0,0,\omega_k);\ f^*_{byk}=f_{byk}(x^*_k,y^*_k,0,0,\omega_k)$$

$$f_{pxk}=f_{pxk}(x_k,y_k,\theta_k,\omega_k);\ f_{pyk}=f_{pyk}(x_k,y_k,\theta_k,\omega_k) \tag{20-25}$$

It is interested to analysis the force components that appear on the right side of Eq. (16) and that will be neglected in the following for the calculation of the modal proprieties. $\{f_p\}$ represents the external forces and torques due to pressure, $\{f_s\}$ is the external torque applied to the driving shaft by the electrical motor and $\{f_b^*\}$ collects constant terms related to bearing reactions evaluated in the SEP. The natural frequency can be estimated solving the following equations of motion obtained from Eq. (16) where the terms on the right side, considered as external forces, and the terms proportional to the velocity have been neglected (normal modes):

$$[M]\{\ddot{q}\}+[K]_L\{q\}=\{0\} \tag{26}$$

The modal properties are obtained by using the GENB pump parameters in Table 1 of this paper and in Table 1 of Part II [2] . Table 2 and Table 3 present the natural frequencies and Figure 3 to Figure 6 depict some modes shapes of the linearized model obtained solving Eq. (26) at different operational conditions. In the linearized equations of motion, the mass matrix is constant at every operational condition while stiffness matrix $[K]_L$ changes with the operational speed and pressure since the bearing stiffness coefficients depend on the SEP and consequently on the output pressure and rotational speed. In the figures representing the mode shapes, the distance between the little circle (undeformed position) and the big circle (deformed position) represents the bending part of the mode, while the torsional part of the mode is represented by the angular shift of the dashed line with respect to the solid line. The results show that the first natural frequency when operated at 34 bar (f_{n1} in Table 2) at each rotational speed represents a bending mode for gear 1 while gear 2 does not show any deformation at every rotational speed (see Figure 3 and Figure 5). Otherwise, the third mode at 34 bar (f_{n3} in Table 2) represents a bending mode for gear 2 whilst gear 1 centre is fix (see Figure 3 and Figure 5). At the operational pressure of 90 bar, the first bending mode for gear 1 is described by the second normal mode (f_{n2} in Figure 4 and Figure 6) and the first bending mode of gear 2 is described by the third normal mode (f_{n3} in Figure 4 and Figure 6). It can be noted that the first bending mode for gear 1 corresponds to a natural frequency lower than the natural frequency of the first bending mode of gear 2. This behaviour is due to the different mass of the gears (gear 1 mass is bigger than gear 2 mass) and to the different bearing stiffness coefficients since they strictly depend on the SEP of the two gears. Moreover, the natural frequencies of corresponding modes, show little changes with the increase of the rotational speed. At 34 bar, the natural frequency increases from 3717 to 3792 Hz when the rotational speed increases from 2000 to 3350 rpm, see Table 2. On the other hand, the frequency variation due to the pressure increment is more relevant: at 2000 rpm, the natural frequency increases from 3717Hz to 5944 Hz when the pressure increases from 34 to 90 bar, see Table 2 and Table 3. This behaviour can be explained as a consequence of the variation of the bearing stiffness coefficients, since they strictly depend on the SEP and on the operational conditions. The natural frequency of 4130 Hz refers to the torsional mode in all the operational conditions. This natural frequency is not affected by

operational conditions since it does not depend on the bearing stiffness coefficients. The torsional mode depends mainly on the torsional stiffness of the gears, and in particular the first torsional mode largely depends on the torsional stiffness of gear 1, being less stiff than gear 2.

4 TEST SET UP AND VALIDATION PROCEDURE

The experimental tests were carried out in a gear pump test bench specifically designed to characterize the noise and vibration behaviour of each unit being tested (Figure 7). Such a test bench is available at TRW Automotive Italia S.r.l. – Division Automotive Pumps. The pump being tested is fastened on an ergal plate (Figure 8) that also provides proper connections to low and high pressure oil pipes. The pump is driven by an electrical motor with inverter having maximum angular speed of 5000 rpm. The plate has a hole for the driving shaft. A Labview based system controls the test bench operation. The plate is equipped with 4 high-impedance quartz-based triaxial force sensors (Kistler 9251, frequency range 1-30000 Hz). These sensors, identified by numbers 1, 2, 3, 4 in Figure 8, allow the user to measure six variables: the three orthogonal X, Y and Z force components and the three moments regarding each coordinate axis. In addition, four PCB 353B18 piezoelectric accelerometers (frequency range 1 to 10000 Hz) are mounted on the plate, as shown in Figure 7(b) and Figure 8 (identified by letters A, B, C, D), in order to measure the plate accelerations in the XY plane. The positive directions of the measured accelerations are +Y', -Y', +X', -X' for accelerometers A, B, C, D, respectively. The eight signals are acquired and processed by LMS hardware and software instrumentation.

Model validation is not a simple task in complex systems like gear pumps where vibration data concerning rotating components are not easy to obtained directly. Therefore, it is necessary to acquire secondary measurements that, after suitable processing, provide quantities that can be compared with simulation results. In the present case, the D'Alembert's equations of the system are considered, where some terms are obtained by means of measurements and others are simulation results. The D'Alembert's principle is applied to the whole system composed of the pump and the force plate, considering the pump casing rigidly fixed to the plate. Only forces and moments in the plane orthogonal to the gear axes are taken into account. The D'Alembert's equations are obtained in the reference frame $O_1X'_1Y'_1$ (Figure 2a and Figure 8) with the origin at the centre O_1 of gear 1 and by evaluating moments about point O_1:

$$\begin{aligned} F_{ecX'} + F_{igX'} + F_{icX'} &= 0 \\ F_{ecY'} + F_{igY'} + F_{icY'} &= 0 \\ M_{ecO_1} + M_{igO_1} + M_{icO_1} &= 0 \end{aligned} \qquad (27\text{-}29)$$

where the sum of all the external force components are:

$$
\begin{aligned}
&F_{ecX'} = R_{X'12} + R_{X'34} \\
&F_{ecY'} = R_{Y'14} + R_{Y'23} - F_P \\
&M_{ecO_1} = \left(R_{X'12} - R_{X'34}\right)\frac{b_2}{2} + \left(R_{Y'14} - R_{Y'23}\right)\frac{b_1}{2} - F_P b_P + M_m
\end{aligned}
\tag{30-32}
$$

Lengths b_1, b_2, b_p are shown in Figure 8. The sum of all the inertia components concerning gears are:

$$
\begin{aligned}
&F_{igX'} = -\left(m_1\ddot{x}_1 + m_2\ddot{x}_2\right)\sin\alpha_w - \left(m_1\ddot{y}_1 + m_2\ddot{y}_2\right)\cos\alpha_w \\
&F_{igY'} = +\left(m_1\ddot{x}_1 + m_2\ddot{x}_2\right)\cos\alpha_w - \left(m_1\ddot{y}_1 + m_2\ddot{y}_2\right)\sin\alpha_w \\
&M_{igO_1} = -\left(a\right)\left(-m_2\ddot{x}_2\sin\alpha_w - m_2\ddot{y}_2\cos\alpha_w\right) - J_1\ddot{\theta}_1 + J_2\ddot{\theta}_2
\end{aligned}
\tag{33-35}
$$

and the sum of all the inertia components concerning the pump casing and force plate are:

$$
\begin{aligned}
&F_{icX'} = -m_{pp}\ddot{x}'_G = -m_{pp}\left(\ddot{x}'_{O_1} + \ddot{\theta}'\,y'_G - \dot{\theta}'^2\,x'_G\right) \\
&F_{icY'} = -m_{pp}\ddot{y}'_G = -m_{pp}\left(\ddot{y}'_{O_1} - \ddot{\theta}'\,x'_G - \dot{\theta}'^2\,y'_G\right) \\
&M_{icO_1} = -J_G\ddot{\theta}' + F_{icX'}\,y'_G - F_{icY'}\,x'_G
\end{aligned}
\tag{36-38}
$$

The second terms within brackets in Eqs (36) and (37) are an order of magnitude lower than the first terms, while the contribution of the normal acceleration components of Eqs. (36) and (37) (terms $\dot{\theta}'^2\,x'_g$ and $\dot{\theta}'^2\,y'_G$) can be neglected. The accelerations of the pump casing and force plate along the X'$_1$ and Y'$_1$ direction (i.e. $\ddot{x}'_{O_1}$ and $\ddot{y}'_{O_1}$ in Eqs. (36) and (37)) and the relative rotational acceleration $\ddot{\theta}'$ can be estimated through the measured accelerations of points A, B, C, D:

$$\ddot{x}'_{O_1} = \frac{\ddot{x}'_C b_D - \ddot{x}'_D b_C}{b_C + b_D}$$
$$\ddot{y}'_{O_1} = \frac{\ddot{y}'_B b_A - \ddot{y}'_A b_B}{b_A + b_B} \qquad (39\text{-}41)$$
$$\ddot{\theta}' = 0.5\left(\frac{\ddot{x}'_C + \ddot{x}'_D}{b_C + b_D} - \frac{\ddot{y}'_A + \ddot{y}'_B}{b_A + b_B} \right)$$

Lengths b_A, b_B, b_C, b_D are shown in Figure 8. The gear inertia components are given by the simulation results in terms of gear accelerations, while the inertia components concerning pump casing and force plate are evaluated by acceleration and force measurements. Regarding the external components, the sensor reactions are measured, the force due to high-pressure pipe F_P are experimental evaluated and the driving shaft torque M_m is given by simulations. It is worth noting that both accelerometers and force sensors have a low frequency limit and do not measure the continuous component. As a consequence, the mean values of all the quantities have to be cancelled, in order to properly compare simulation and test results. Thus, the mean value of the driving shaft torque M_m is cancelled and the high-pressure pipe force (F_P) is not considered, since the pressure variation around its mean value gives a negligible contribution with respect the other components.

Thus, reorganizing Eqs. (27) to (29) in order to put the terms given by measurements on the left side and the terms given by simulation on the right side, the following equations are obtained:

$$R_{X'12} + R_{X'34} + F_{icX'} = -F_{igX'}$$
$$R_{Y'14} + R_{Y'23} + F_{icY'} = -F_{igY'} \qquad (42\text{-}44)$$
$$\left(R_{X'12} - R_{X'34}\right)\frac{b_2}{2} + \left(R_{Y'14} - R_{Y'23}\right)\frac{b_1}{2} + M_{icO_1} = -M_{igO_1} - M_m$$

It is worth noting that the terms on the right side of Eqs. (42) to (44) are the opposite of the inertia and external components directly acting on the gears. These components load the pump casing and the plate and produce the reactions and the inertia forces on the left side. In operational conditions these are the components that can excite casing vibrations and produce noise. Consequently, their estimation has a practical interest. In the following section the validation is carried out comparing the experimental data on the left side and the simulation data on the right side of Eqs. (42) to (44).

5 VALIDATION RESULTS

The validation is carried out using data both in the time and in the frequency domain. The model parameters were preliminarily evaluated on the basis of both design and literature data. The values of damping factors γ_T and γ_m (proportionality constant between viscous damping coefficient and stiffness of a tooth pair and of the driving shaft, respectively) are adjusted in order to better match experimental results. Table 1 lists the values of the model parameters.

The validation results in the time domain concern operational pressures of 34 and 90 bar and angular speeds of 2000 and 3350 rpm. The time histories of the experimental forces and accelerations on the left side of Eqs. (42) to (44) were acquired using sampling frequency of 51.2 kHz and frequency resolution 1.56 Hz, while the gear accelerations and the shaft torque were computed by means of the model for a time corresponding to 48 meshing periods T, using display frequency of 48 kHz. Since the main harmonics in the acceleration spectrum lie in the frequency range till 7kHz, both experimental and simulation quantities were digitally filtered at 7 kHz.

The time domain comparison has been carried out by taking advantage of the the Time Synchronous Average (TSA). TSA [22,23] is a common method used to process the signal in presence of rotational element. It consists in the synchronization of the sampling for the measured signal with the rotational element of interest, and the evaluation of the ensemble average over many revolutions with the start of each frame at the same angular position. In this way a signal called TSA is obtained, which in practice contains only the components synchronized with the rotational element in question. If sufficient averages are taken, the TSA closely approximates a truly periodic signal with periodicity corresponding to one revolution of the selected rotational element. This process strongly reduces the effect of components non-synchronous with the reference. Moreover, measurement noise is reduced too. The TSA has been performed in post-processing with a linear interpolation method, which permits to resample the signal using a fixed number of samples per revolution [23].

The time synchronous average (TSA) of the experimental quantity on the left side of Eqs. (42) to (44) was computed over 250 meshing periods at 2000 rpm and 400 meshing periods at 3350 rpm, while the TSA of the simulation quantity on the right side was computed over 48 meshing periods. Figure 9 shows the comparison between the experimental RMS values of the TSA and the simulation ones. The agreement between the RMS values is not satisfactory at 3350 rpm - 90 bar in X'-direction and at 3350 rpm - 34 bar in Y'-direction, but in the other operational conditions and

directions the agreement is rather good. This indicates that the model is able to give a satisfactory evaluation of the variable forces and thus of the gear accelerations.

The validation results in the frequency domain concern two linear run-up tests from 2000 to 3350 rpm, with operational pressure of 34 bar and 90 bar respectively, carried out with the apparatus described in the previous section. The run-ups were acquired using sampling frequency of 25.6 kHz and frequency resolution of 3.125 Hz. During the run-up tests, 67 spectra of the quantity on the left side of Eqs. (42) to (44) were acquired. These spectra are taken at speed intervals of 20 rpm between 2000 to 3350 rpm and they are shown as waterfall maps in Figure 10 to Figure 12. In order to compare simulation data with the experimental run-ups, 27 simulations were conducted at the operational pressure of 34 bar and 90 bar and angular speed interval of 50 rpm from 2000 to 3350 rpm. The simulations were carried out for a time corresponding to 48 meshing periods T, using display frequency of 48 kHz. The simulation time (48 meshing periods T) is variable due to the variation of the rotational speed (from 2000 to 3350 r.p.m.). Since the frequency resolution is the invers of the simulation time, the frequency resolution is variable for each of the 27 simulations. It is a matter of fact that the meshing period equals to $60/nz_k$, where n denotes the gear velocity in r.p.m. and z_k is the tooth number of gear k (z_k =12 for this gear pump). At 2000 r.p.m. the meshing period is 0.0025s and the simulation time is 48*0.0025=0.12s; therefore the frequency resolution is 8.3Hz. At 3350 r.p.m. the meshing period is 0.0015s and the simulation time is 0.072s; therefore the frequency resolution is 14 Hz.

For each simulation the quantity on the right side of Eqs. (42) to (44) was evaluated and its frequency spectrum was calculated. Figure 10 to Figure 12 show these amplitude spectra as waterfall maps in the frequency range till 7000Hz. It is worth noting that the experimental and simulation spectral maps have different resolution: the frequency resolution is 3.125 Hz for experimental spectra and for the simulation ones ranges from 8.3 to 14 Hz, as highlighted above; the resolution in the rpm-axis is 20 rpm for the experimental spectra and 50 rpm for the simulation ones. The amplitude grey scale is the same for the pairs of maps relative to the same direction and operational conditions. Since the comparison regards a wide frequency range (till 7000Hz), the difference in terms of frequency resolution between the experimental and numerical maps does not reduce the validity of the comparison. It can be useful to compare the natural frequencies and mode shapes of the corresponding undamped linearized model (Section 3) with the experimental resonances exhibited in the waterfall maps. The experimental waterfall maps (Figure 10 to Figure 12) show some resonance regions: from about 500 Hz to 2.5 kHz in X’ and Y’-directions and at about 3.4 kHz, 4.2 kHz, and 5.2 kHz in all the components. At the operational pressure of 34 bar, the experimental resonances at about 3.4 kHz, 4.2 kHz, 5.2

kHz satisfactorily agree with the natural frequencies estimated by the linearized model (Table 2). At high pressure (90 bar), the first two natural frequencies of the model (Table 3) can be found in the experimental waterfall maps. In the other frequency ranges, a quite good correspondence in the X'-direction maps at both pressure levels, while discrepancies occur in the Y'-direction maps. The correspondence is good in the momentum maps, especially around the resonances at about 4.2 kHz. Further research is needed in order to understand the causes of the discrepancies (especially in Y'-direction at high pressure) and to adjust the model. The discrepancies between experimental and simulation results could be also due to the approximations introduced in Eqs. (42) to (44), when it has been considered that the pump casing is rigidly fixed to the plate and that the pressure variations of the high-pressure pipe are negligible. Other causes of discrepancy can be imputed to the pump casing dynamics which is not considered and other sources of excitation as the electrical motor, the test bench, the fluid dynamics of the output ducts.

In Part IV, the model will be improved leading to better validation results.

6 MODEL EXTENSION TO HELICAL GEAR PUMPS

Once the model has been validated and its effectiveness satisfactory proved, it can be modified and used in order to study the dynamic behaviour of a new prototype of gear pump. The assessed model could be used as a tool for design optimization. In particular, the model can calculate the variable forces exiting the pump casing, estimate the gear centre trajectory and the gear accelerations. With regard to this, the assessed model is adapted to a new virtual prototype, namely *GENB_P* in view of evaluating gear accelerations and variable forces before the hard prototype is available.

6.1 Model modifications

This new pump has helical gears, while the previous one has spur gears. The use of helical gears introduces an axial force that must be taken into account for the definition of the pressure compensation along the axial direction. Moreover, if the helical angle increases, the inlet and outlet chambers will be connected for more time reducing the hydraulic efficiency. As a consequence, the helical angle cannot be higher than six degrees for this kind of application. This situation allows us to assume that the axial forces are negligible and therefore the gear pump can be modelled using the same planar model of the previous gear pump (GENB). The assumption of planar model is also acceptable for the new *GENB_P* pump due to the helix angle of 4 deg. Table 1 summarizes the main characteristics of the new *GENB_P* and of

the GENB pump. The main difference of the new *GENB_P* pump compared to the GENB pump refers to gears: the twin gears have 11 teeth with helix angle of 4 deg.

Three main modifications in the original model have to be performed: the geometrical data, the meshing stiffness formulation for helical gears, the phase difference between the lower and upper tooth surfaces in contact with the bearing blocks. Since the code of the presented elastodynamic model has a pre-processing module for input data introduction, the geometrical data updating is simple and fast. The consequence of the phase difference between the lower and upper tooth surfaces of helical gears is explained hereafter. The beginning of the connection between the trapped volume and the inlet chamber happens at the same instant as in case of spur gears. On the other hand, the end of the connection with the outlet chamber is postponed. This delay is due to the helix angle. As a matter of fact, a spur gear can be studied as a planar system, because its behaviour is the same in all the axial sections of the gear. Otherwise, in helical gears, any axial sections of the gear are always out of phase and between the tooth upper surface and the tooth lower surface, the phase difference is maximum. Such a phase difference is directly dependent on the helix angle. With reference to Figure 13(a), when the contact point on the tooth upper surface intersects the relief grooves, the connection between the trapped volume and the outlet chamber is closed only in the upper surface, but it is still opened in the lower one, up till the contact point on the tooth lower surface intersects the relief grooves, as shown in Figure 13(b). In order to model such a behaviour, i.e. in order to postpone the end of the connection with the outlet chamber, the base pitch of the gears has been artificially increased by quantity $\Delta P_b = b\tan\left(\beta_b\right)$, where β_b is the helix angle calculated on the base circle:

$$\beta_b = \tan^{-1}\left(\frac{r_{bk}\tan\left(\beta\right)}{R_{pk}}\right). \tag{45}$$

With reference to Figure 14, the seal line is the segment of the line of action limited by the intersections with the relief grooves ($\overline{CD} = \dfrac{B}{\cos(\alpha_w)}$). The percentage difference (*%diff*) between the seal line and base pitch P_b indicates the percentage of the meshing period in which the inlet and outlet chambers are in communication. For spur gear GENB pump, this percentage is:

$$\%diff_{GENB} = \frac{\frac{B}{\cos(\alpha_w)} - P_b}{P_b} 100 = -3.50\% \tag{46}$$

For helical gear GENB_P pump, the contemporaneous communication between the inlet and outlet chamber is increased by the base pitch increment (ΔP_b) as:

$$\%diff_{GENB\_P} = \frac{\frac{B}{\cos(\alpha_w)} - (P_b + \Delta P_b)}{P_b} 100 = -3.52\% \tag{47}$$

A similar problem happens when a new tooth space becomes isolated in the inlet side. For gear 1, at the inlet port, a tooth space becomes isolated later with respect to a spur gear, due to the phase difference between the upper and lower surfaces of the tooth in helical gears. Taking Figure 14(a) as a reference, the first tooth space becomes completely isolated at the inlet side not when the tooth upper surface goes beyond the line identified by angle Φ_{B1} but when the tooth lower surface goes beyond such a line (see Figure 14(b)). Therefore, in order to take such a delay at the inlet port into account, angle Φ_{B1} has been decreased by a quantity equal to the above phase difference. The same happens for gear 2 at the inlet port. So in the updated model, angle Φ_{B2} has been decreased by the same quantity as angle Φ_{B1}. At the output side, the behaviour of the helical gears and spur gears is identical, therefore no modifications are needed. The last modification that has to be taken into account regards the meshing stiffness. Among the stiffness approaches available in the literature, the Cai's formulation was selected [24][25]. Such a theory proposes to consider the helical gears as a planar system and introduces the helical effect by a stiffness function smoother than the stiffness function in case of spur gears:

$$K(t) = \bar{k} \exp(C_\beta \left|\bar{s}(t)\right|^3) \tag{48}$$

where $\bar{k}$ is the stiffness value at the pitch point [N/m] accounting the gear width , C_β is a constant linearly related to helix angle β and $\bar{s}(t)$ is a dimensionless time-dependent function that defines the position of the meshing contact

along the line of action. Then, the total stiffness of the tooth pair is obtained considering also the Hertzian stiffness contribution.

6.2. Simulation results and discussion

Hereafter the model for helical gear pumps has been used in order to identify the physical events that determine sudden variations on forces and torques and therefore on the dynamic response of the system (gear accelerations). The events due to dynamic phenomena are: change in number of meshing teeth (from 1 to 2 and 2 to 1), change in number of isolated tooth spaces carrying fluid for gear 1 and 2 (from 5 to 6 and 6 to 5) and finally beginning and ending of the trapped volume connection with the input and output volume. Since the hard prototype of the *GENB_P* was not available, obviously, the profile error trend cannot be measured. Therefore, the simulation results are obtained neglecting the terms related to profile errors. Figure 15 shows the events causing high peaks on gear accelerations at the operational condition of 3350 rpm and 34 bar. It can be noted that the phenomena producing the most important dynamic effects are the increment in the number of isolated tooth spaces (from 5 to 6) and the events related to the trapped volume. Variable meshing stiffness has a notable effect as well, but not as important as the trapped volume. In the following, the simulation results of the *GENB_P* and *GENB* pumps will be compared in terms gear accelerations and pressure forces (Figure 16 and Figure 17) at the operational condition of 2000 rpm and 90 bar. The pressure forces (Figure 16) show higher values (in absolute value) for the *GENB_P* pump with respect to the GENB. Nevertheless, the gear accelerations (Figure 17) have similar peak values even if the maximum level of the GENB accelerations is higher than in the *GENB_P* pump. It is worth noting that the acceleration trends are different because the events that determine the force variation occur in different instants, due to the different geometry of the new prototype. Finally, since the helix angle β_b of the *GENB_P* is equal to 3.708 deg, the axial component $f_{mg,axial}$ of the meshing force is

$$f_{mg,axial} = f_{mg} \sin(\beta_b) = 0.0646\, f_{mg} \tag{49}$$

that is to say that $f_{mg,axial}$ is about 6% of the global meshing force f_{mg} acting along the line of action. Furthermore, neglecting the inertial contribution and damping effects, the driven gear is unloaded in axial direction because the axial pressure force has similar amplitude but opposite direction of the axial meshing force. On the contrary the driving gear is loaded by $2 f_{mg,axial}$ in axial direction, because the axial pressure force has same amplitude and direction as the axial meshing force.

7. CONCLUDING REMARKS

This work concerns the experimental validation of a kineto-elatodymanic model of external gear pumps. It is a non-linear lumped-parameter model, which takes into account the variability of the pressure distribution on gears, the hydrodynamic bearing behaviour, the parametric excitation due to gear meshing and tooth profile errors, the effects of the backlash between meshing teeth, the lubricant squeeze and the possibility of tooth contact on both lines of action. In order to reduce the numerical integration time, the pressure distribution is preliminary estimated for the 'static' position of the gears. The non-linear model includes all these important dynamic effects, in order to take into account and analyse their interactions. An experimental apparatus has been set up for the measurements of the accelerations and the force components applied to the pump casing in operational conditions. A novel validation procedure has been proposed based on the comparison between simulation and experimental results concerning forces and moments: it deals with the external and inertia components acting on the gears, estimated by the model, and the reactions and inertia components on the test plate and the casing, obtained by means of measurements. These are the components that can excite casing vibrations and produce noise; consequently, their estimation also has a practical interest for noise reduction.

The validation results concerning the RMS values of the time synchronous average can be considered rather good. This indicates that the model is able to give a satisfactory evaluation of the force levels exciting the casing. The validation results in the frequency domain was carried out by comparing the resonances region exhibited by the experimental waterfall maps with the natural frequency of the linearized model and the simulation waterfall maps. The first natural frequencies of the linearized model can be found in the experimental maps, while the correspondence between the experimental and simulation maps is good in some cases and worse in others. In view of all the validation results, the correspondence between simulations and tests can be considered rather satisfactory, taking into account the complexity of the model including several non-linear dynamic phenomena. Although the model validation concerns a particular gear pump, the procedure has a general meaning and it can be used in similar applications or mechanical systems, when the measured vibration data concerning rotating components are difficult to directly obtained.

As an example of application, the assessed model has been properly modified in order to evaluate gear accelerations and dynamic forces of a new virtual pump prototype with helical gears. On the basis of the numerical simulations it is possible to drawn the following remarks: i) the variable meshing stiffness has a minor contribution with respect to the other dynamic events that occurs along the meshing period, in terms of acceleration peaks; ii) the amplitude of the

pressure forces has higher values in the helical gear pump than those in the spur gear pump, nevertheless, the gear accelerations have similar peak values even if the maximum level of the spur gear pump accelerations is higher than in the helical gear pump; iii) due to the helical gears, the driving gear of the helical gear pump is loaded in axial sense with a load of about 12% of the meshing force. Thus, the model can be a very useful tool in prototype design and in order to develop design improvements for NVH optimization.

ACKNOWLEDGEMENTS

The authors wish to thank TRW Automative Italia S.r.l. – Division Automotive Pumps (Ostellato, Ferrara, Italy) and the engineers of this Company for co-operation and assistance in the collection of model data. This work has been developed within the Advanced Mechanics Laboratory (MechLav) of Ferrara Technopole, realized through the contribution of Regione Emilia-Romagna - Assessorato Attivita' Produttive, Sviluppo Economico, Piano telematico - POR-FESR 2007-2013, Attività I.1.1..

REFERENCES

[1] E. Mucchi, G. Dalpiaz, A. Fernàndez del Rincòn, Elasto-dynamic analysis of a gear pump. Part I: pressure distribution and gear eccentricity, Mechanical Systems and Signal Processing 24 (2010) 2160-2179.
[2] E. Mucchi, G. Dalpiaz, A. Rivola, Elasto-dynamic analysis of a gear pump. Part II: Meshing phenomena and simulation results, Mechanical Systems and Signal Processing 24 (2010) 2180-2197.
[3] J.M. Réveillé, Progress in automotive NVH field, Proceedings of International Conference on Noise and Vibration Engineering, Leuven, Belgium, 2002 September 16-18, Leuven (2002).
[4] I. M. Bidhendi, K. Foster, R. Taylor, Computer predictions of cyclic excitation sources for an external gear pump, Computer Aided Design in High Pressure Hydraulic Systems Symposium, ImechE, 1983.
[5] H. Nevzat Ozguven, D. R. Houser, Mathematical Models Used in Gear Dynamics – A review, Journal of Sound and Vibration 121/3 (1988) 383-411.
[6] J.D. Smith, Gear noise and vibration, Marcel Dekker, Inc. 1999.
[7] P. Velex, M. Maatar, A mathematical model for analyzing the influence of shape deviations and mounting errors on gear dynamics behaviour, Journal of Sound and Vibration 191/5 (1996) 629-660.
[8] H. Nevzat Ozguven, D.R. Houser, Dynamic analysis of high speed gears by using loaded static transmission error, Journal of Sound and Vibration 125/1 (1988) 71-83.
[9] C. Bonacini, M. Borghi, Calculation of the pressures in the vanes between teeth of an external gear, Oleodinamica-pneumatica (1991) (in Italian).
[10]M. Borghi, M. Milani, F. Paltrinieri, B. Zardin, Pressure transient in external gear pumps and motors meshing volumes, 2005 SAE international, 2005-01-3619.
[11]S. Mancò, N. Nervegna, Simulation of an external gear pump and experimental verification, Proceedings of the International symposium on fluid power, Tokyo, March 1989.
[12]S. Theodossiades, S. Natsiavas, On geared rotordynamic systems with oil journal bearings, Journal of Sound and Vibration, Vol. 243 No.4, Academic Press (2001), pp 721-745.
[13]G. Ceptureanu, S. Nedelcu, Sliding bearings, V.N.Constantinescu, A. Nica, M. D. Pascovici, Allerton Press, Inc./New York,1985.
[14]A. Seireg, Friction and lubrication in mechanical design, Marcel Dekker, Inc.,1998.
[15]F. Patrinieri, M. Milani, M. Borghi, Modelling and simulation hydraulically balanced external gear pumps, Proceedings of the 2nd International FPNI Ph.D. Symposium on Fluid Power, Modena (Italy), 3-6 July, 2002.
[16]G. Miccoli, P. Vagnoni, Experimental determination of casing loads on an external gear pump, Oleodinamica-pneumatica, Novembre 1988, pp. 145-155 (in Italian).
[17]H. Yanada, T. Ichikawa, Y. Itsuji, Study of the trapping of fluid in a gear pump, Imeche 1987, Vol. 201, pp. 39-45.

[18]J.H. Kuang, Y.T. Yang, An estimate of mesh stiffness and load sharing ration of a spur gear pair, Proceedings of the International Power Transmission and Gearing Conference Vol. 1, Scottsdale, Arizona, 1992 1-9.

[19] Mancò S., Nervegna, N. *Pressure Transients in an External Gear Hydraulic Pump, proceedings of the* Second JHPS (Japan Hydraulics and Pneumatics Society) International Symposium on Fluid Power, Tokyo, Japan, Sept 1993".

[20]D. Childs, H. Moes, H. Van Leeuwen, Journal bearing impedance descriptions for rotordynamic application. Journal of lubrication technology 99 (1977) 198-214.

[21] Rotordynamics of Turbomachinery, John M. Vance, John Wiley & Sons, 1988.

[22]M. Malagò, E. Mucchi, G. Dalpiaz, Condition Monitoring and Diagnostics in Heavy-Duty Wheels: a First Experimental Approach, Proceedings of the ASME 2009 International Design Engineering Technical Conferences & Computers and Information in Engineering Conference, August-September 2009.

[23]Fyfe K. R., Munck D. S., Analysis of computed order tracking, Mechanical System and Signal Processing 11/2 (1997) 187-205.

[24] Y. Cai, Simulation on the rotational vibration of helical gears in consideration of the tooth separation phenomenon (A new stiffness function of helical involute tooth pair), Journal of Mechanical Design,177 (1995) 460-469.

[25] Y. Cai, Development of a silent helical gear reducer (Vibration simulation and noise measurement), Proceedings of the Power Transmission and Gearing Conference, Vol. 88, San Diego, California, 1996.

FIGURES

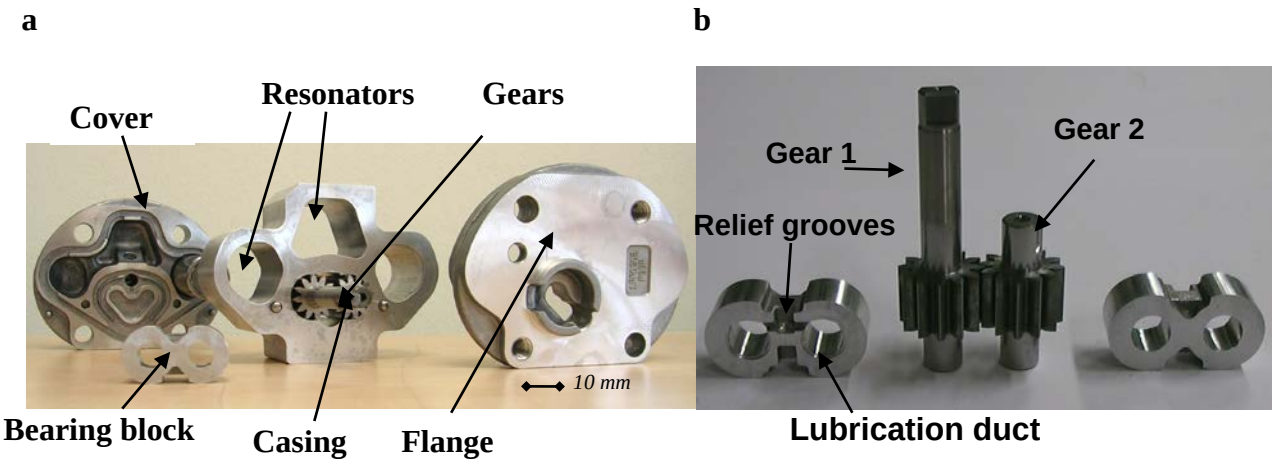

Figure 1. a) Enlarged photo and b) details on gears and bearing blocks.

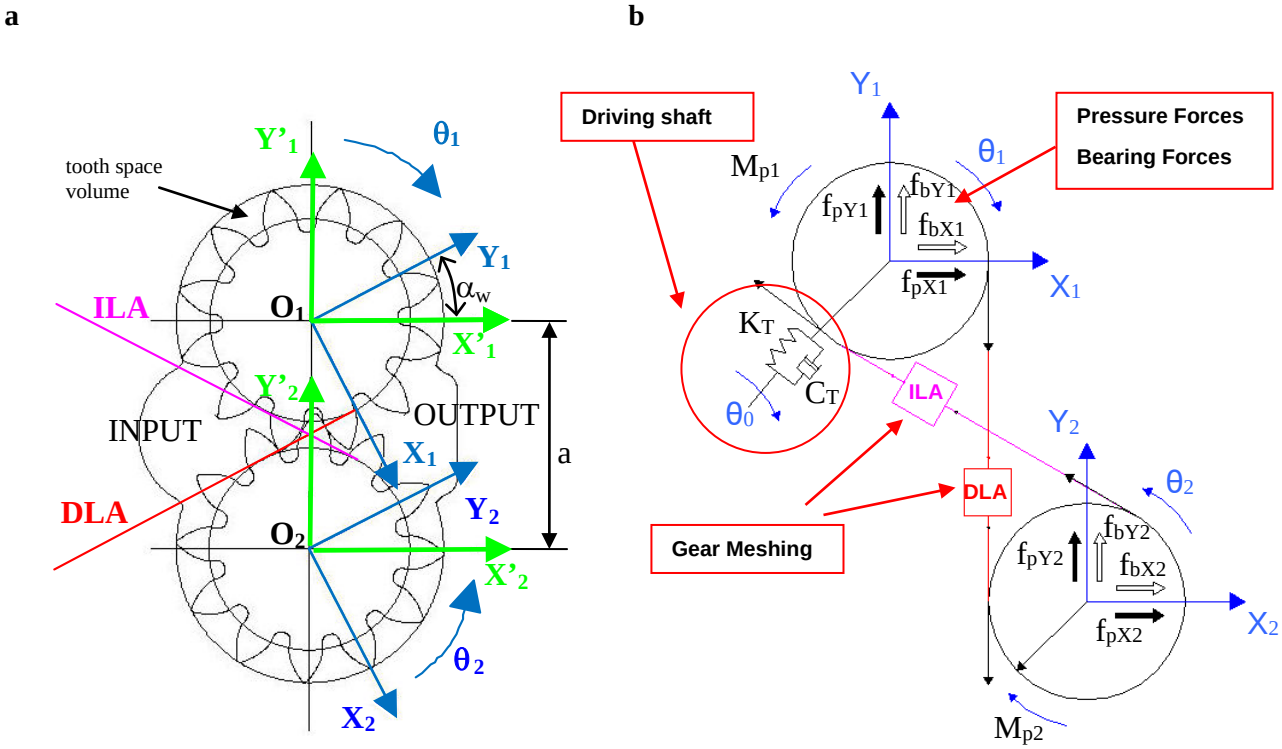

Figure 2. (a) Reference frames and (b) diagram of the model.

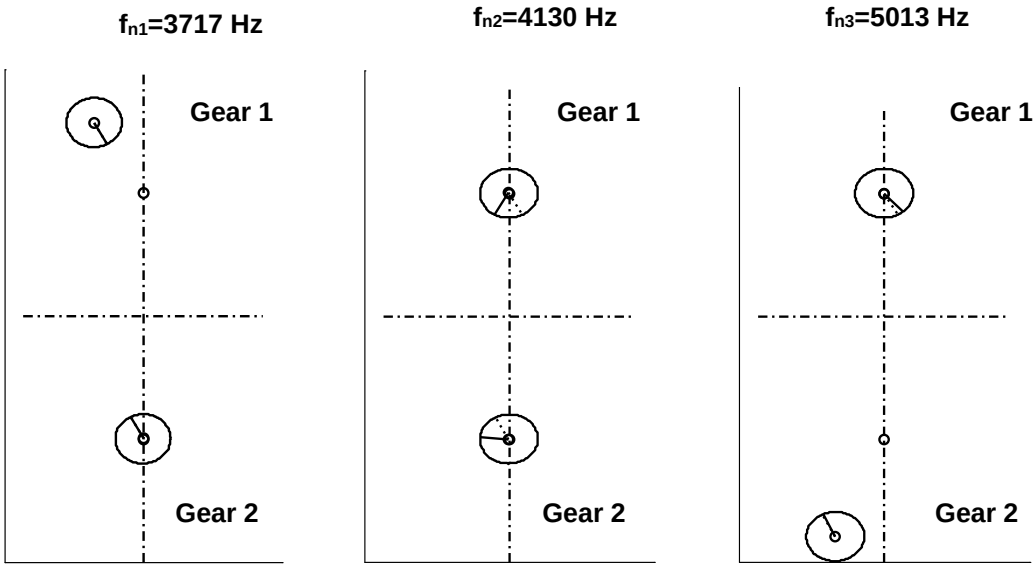

Figure 3. First three mode shapes at 2000 rpm and 34 bar. The blue circle represents gear 1 and the red one represents gear 2. From left to right, bending mode of gear 1, torsional mode and bending mode of gear 2.

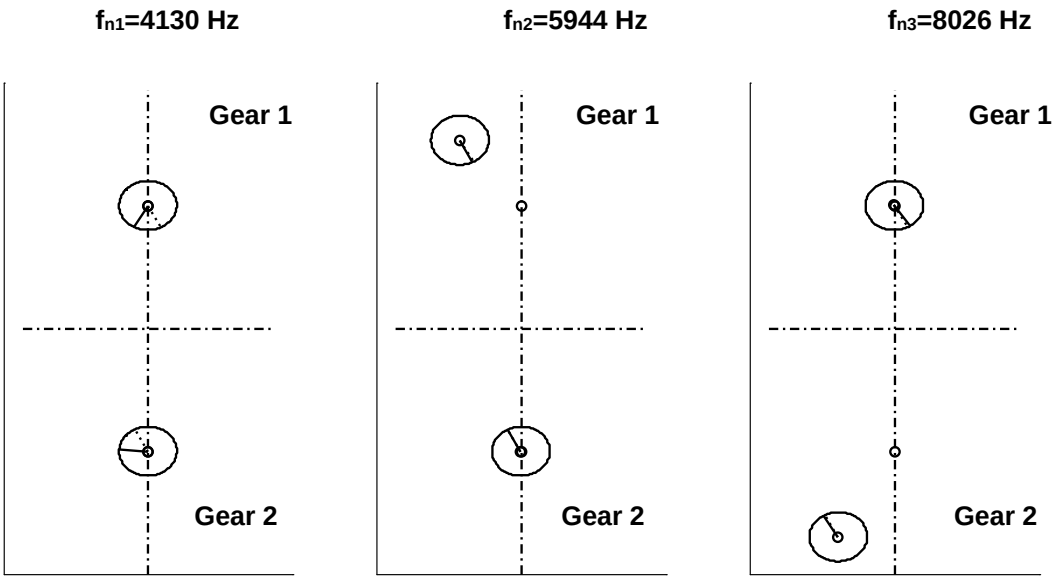

Figure 4. First three mode shapes at 2000 rpm and 90 bar. The blue circle represents gear 1 and the red one represents gear 2. From left to right, torsional mode, bending mode of gear 1 and bending mode of gear 2.

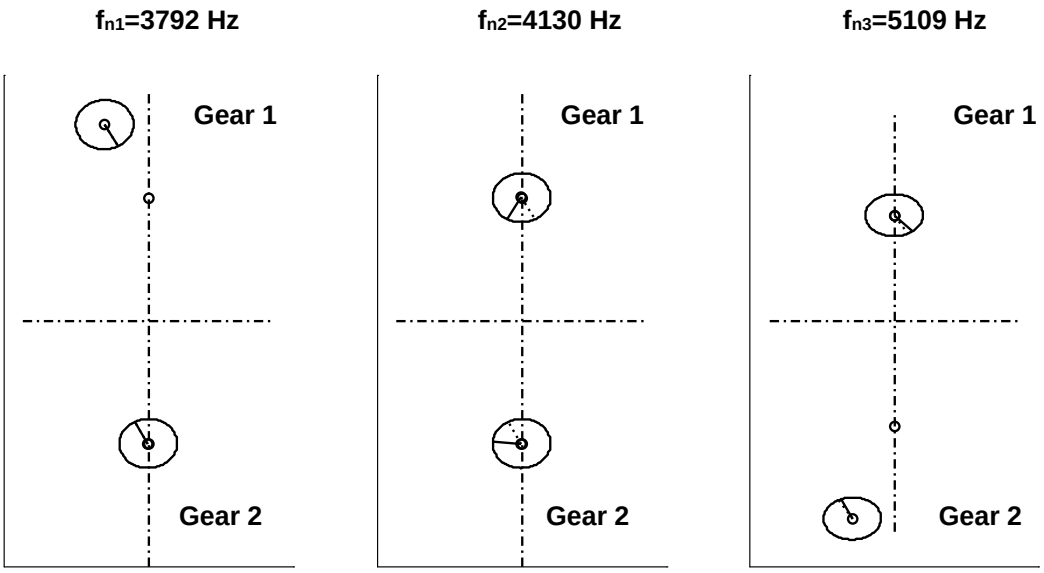

Figure 5. First three mode shapes at 3350 rpm and 34 bar. The blue circle represents gear 1 and the red one represents gear 2. From left to right, bending mode of gear 1, torsional mode and bending mode of gear 2.

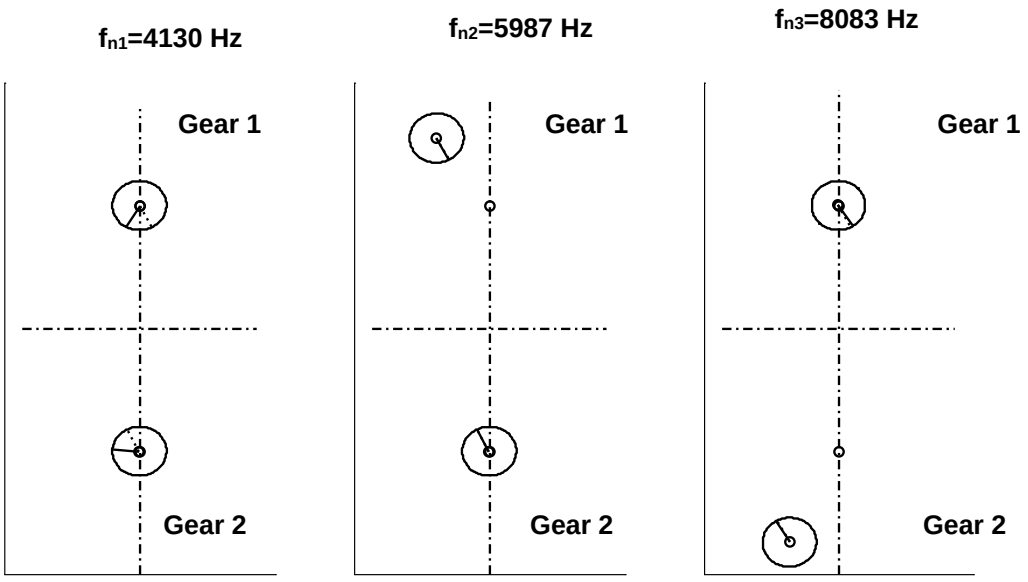

Figure 6. First three mode shapes at 3350 rpm and 90 bar. The blue circle represents gear 1 and the red one represents gear 2. From left to right, torsional mode, bending mode of gear 1 and bending mode of gear 2.

a **b**

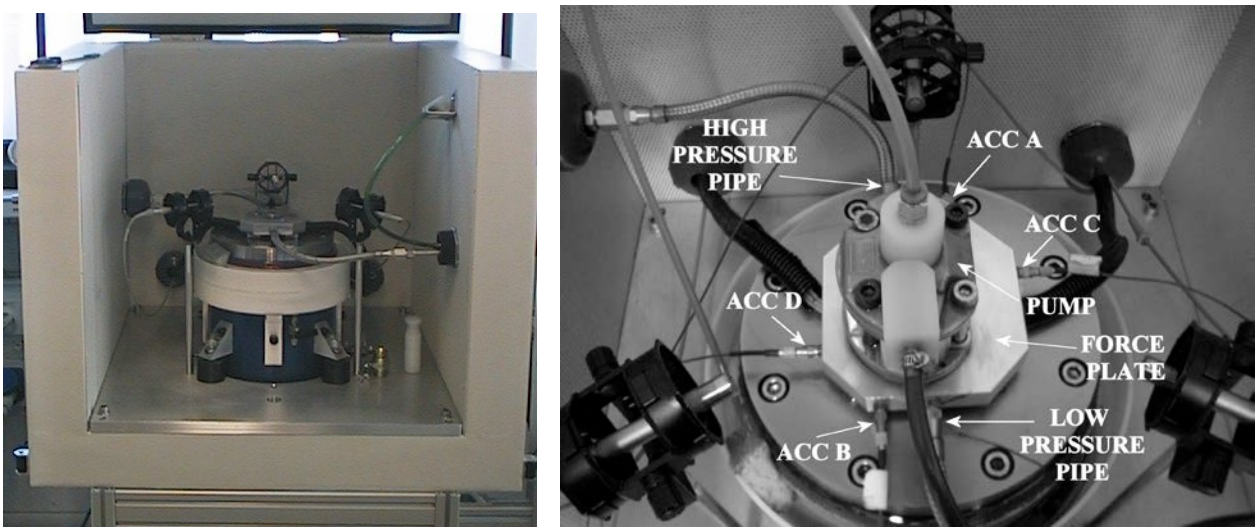

Figure 7. (a) Test bench and (b) pump being tested.

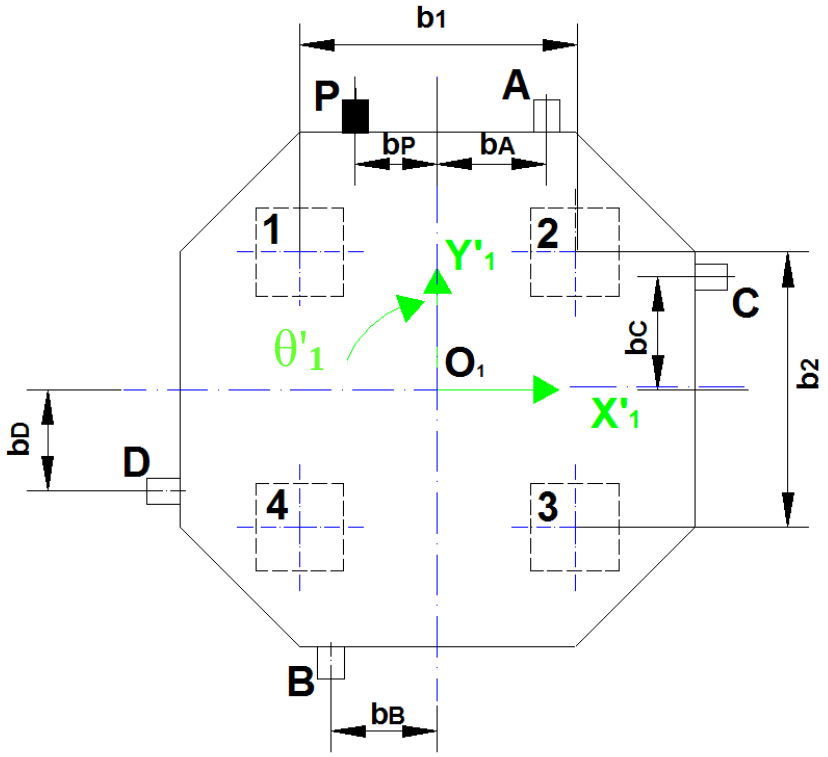

Figure 8. Schematic of the force plate with the reference frame: locations of force sensors (1, 2, 3, 4), accelerometers (A, B, C, D) and high pressure pipe (P).

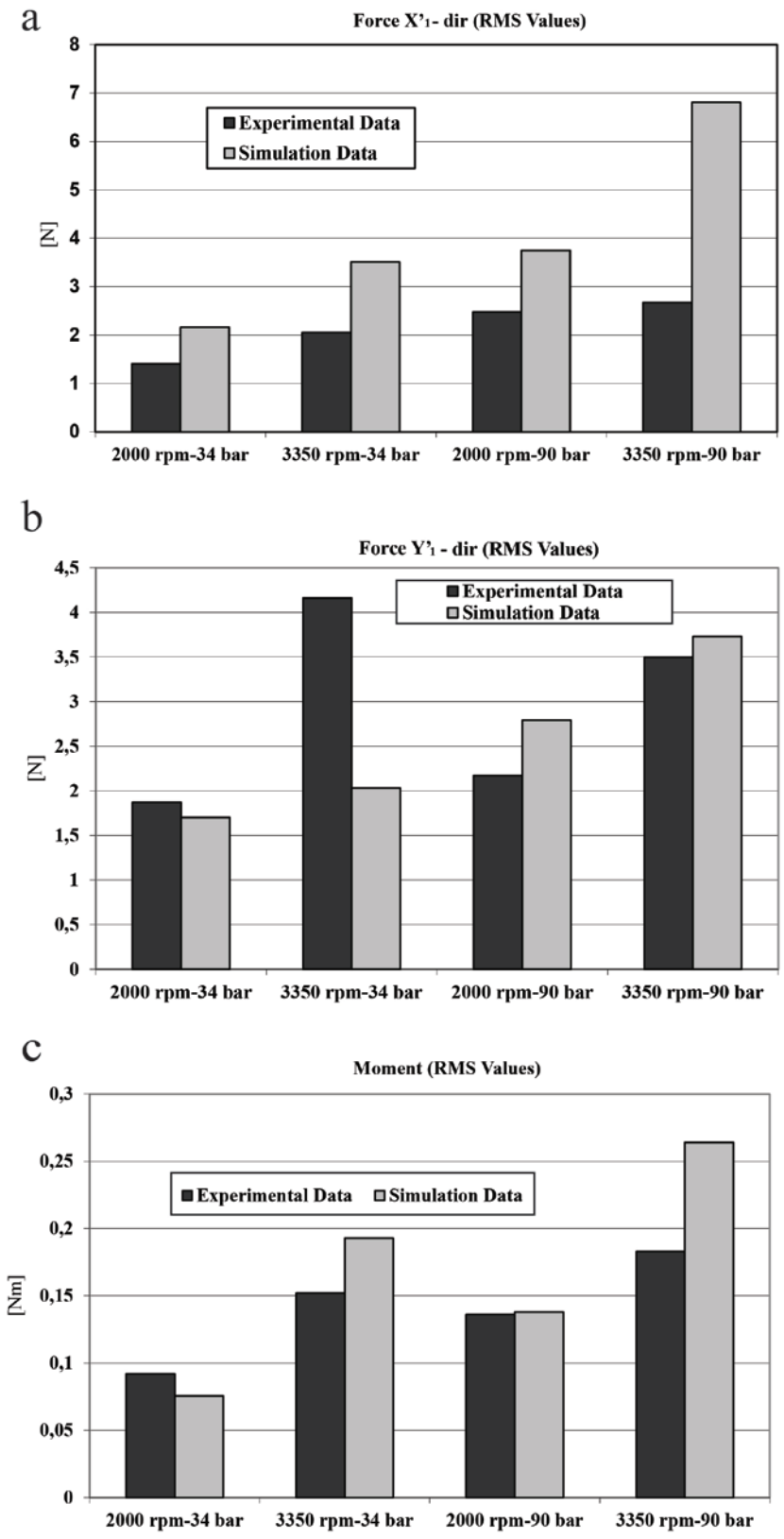

Figure 9. RMS values of the TSA relative to one meshing period of (a) force in $X_1^{'}$-direction, (b) force in $Y_1^{'}$-direction, (c) moment about point O_1 in $\theta_1^{'}$-direction.

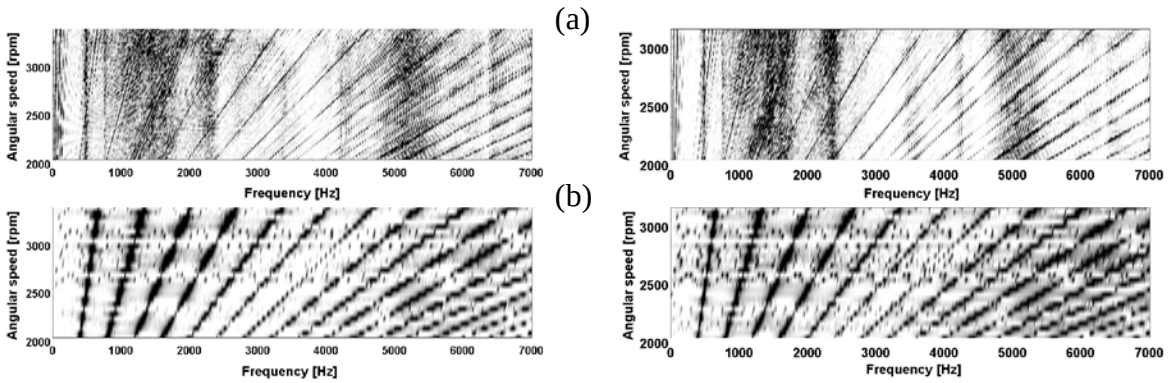

Figure 10. Waterfall maps of force spectra in $X_1^{'}$-direction at 34 bar (left) and 90 bar (right); according to the experiment (a) and simulation (b).

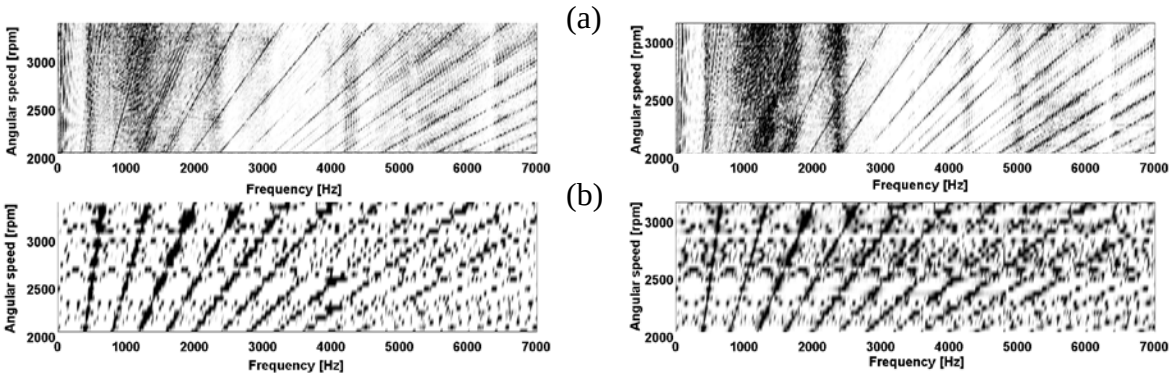

Figure 11. Waterfall maps of force spectra in $Y_1^{'}$-direction at 34 bar (left) and 90 bar (right); according to the experiment (a) and simulation (b).

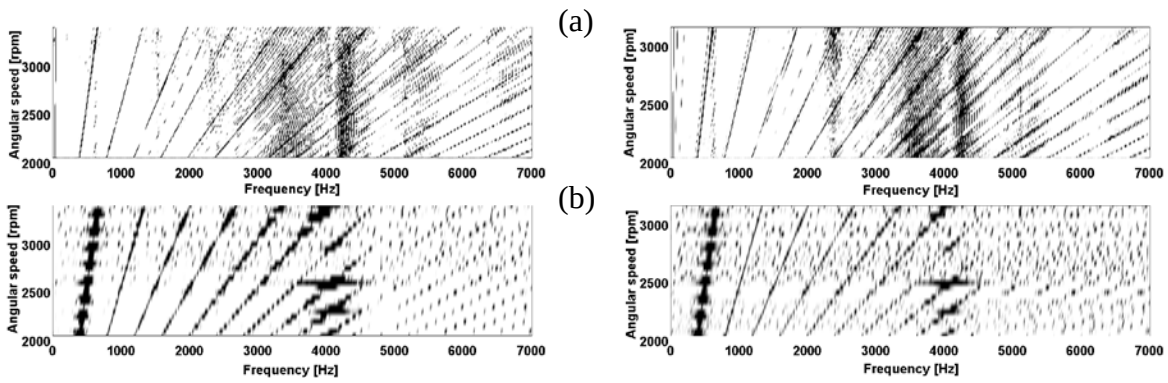

Figure 12. Waterfall maps of moment spectra (θ'_1-direction) at 34 bar (left) and 90 bar (right); according to the experiment (a) and simulation (b).

a

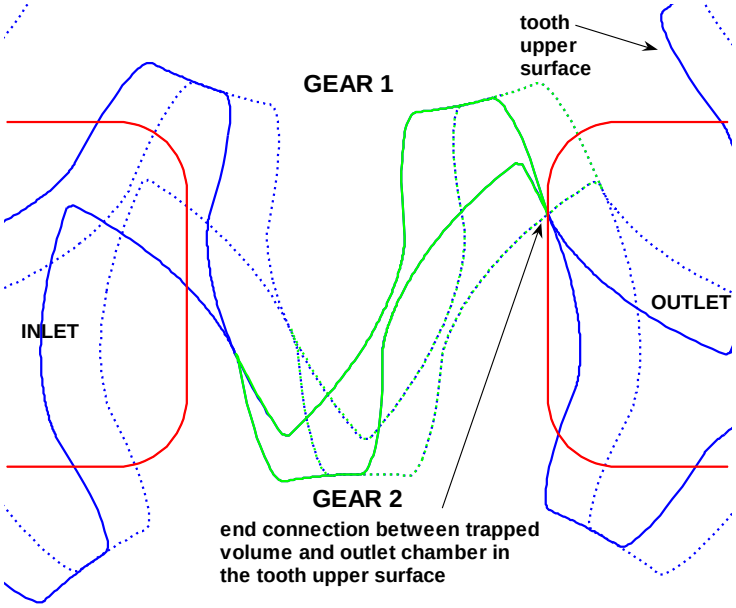

b

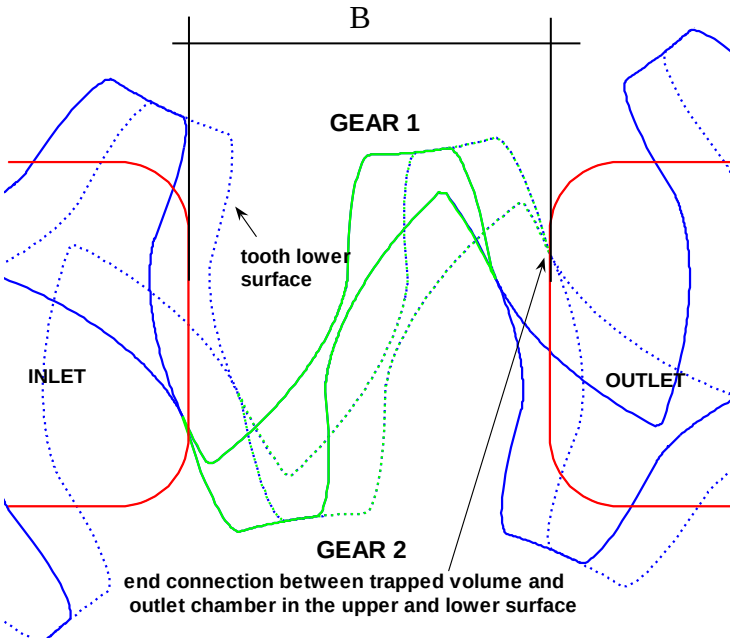

Figure 13. (a) End of the connection between trapped volume and outlet chamber in the tooth upper surface, (the connection is still open in the lower surface, in dotted line) and (b) end of the connection between trapped volume and outlet chamber in the tooth upper and lower surfaces.

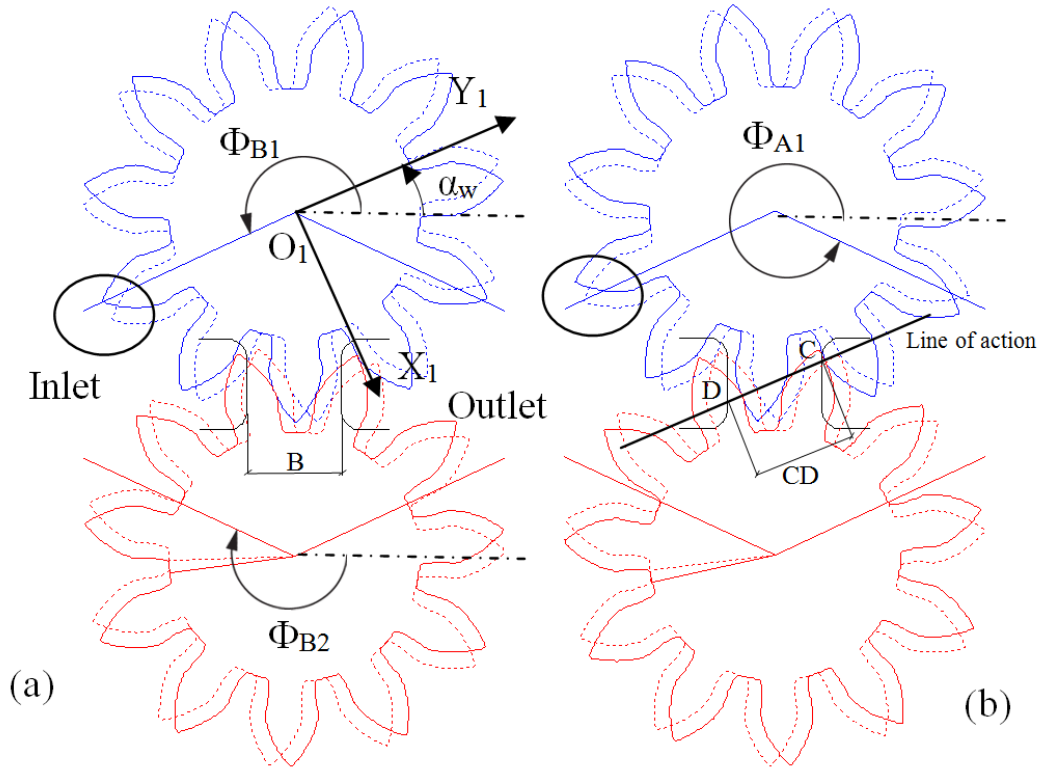

Figure 14. (a) The upper surface of gear 1 (in blue) goes beyond the Φ_{B1} line and (b) the lower surface of gear 1 goes beyond the Φ_{B1} line and the first tooth space becomes completely isolated (the lower surface is in dotted line and the upper in solid line).

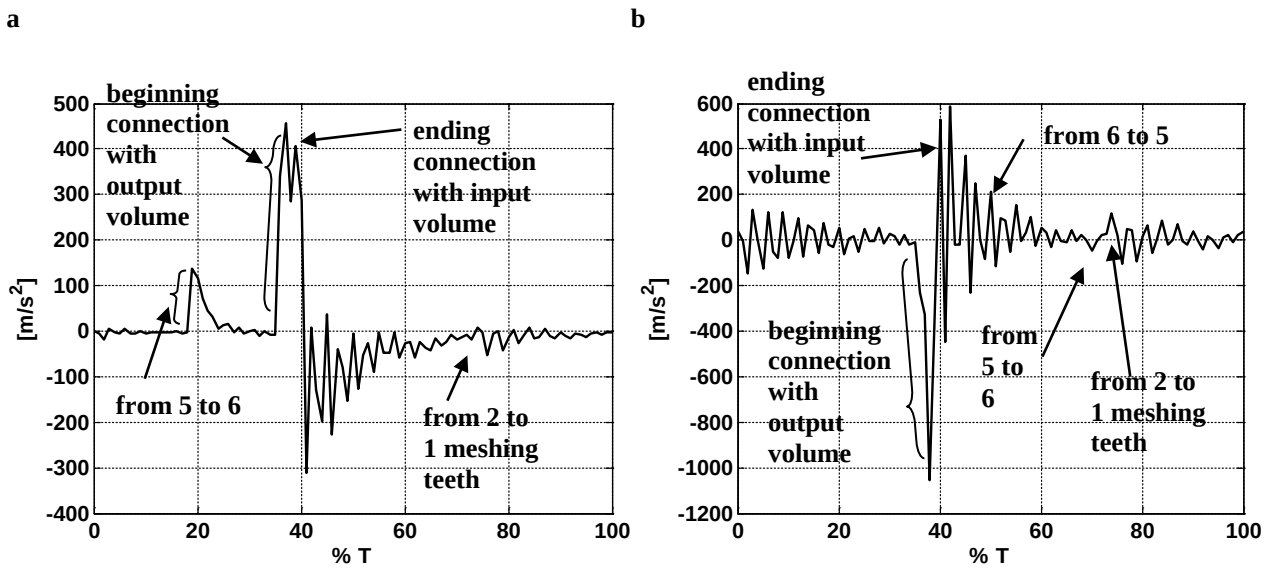

Figure 15. Accelerations of (a) gear 1 and (b) gear 2 in X_1-direction, over one meshing period; operational condition of 3350 rpm and 34 bar.

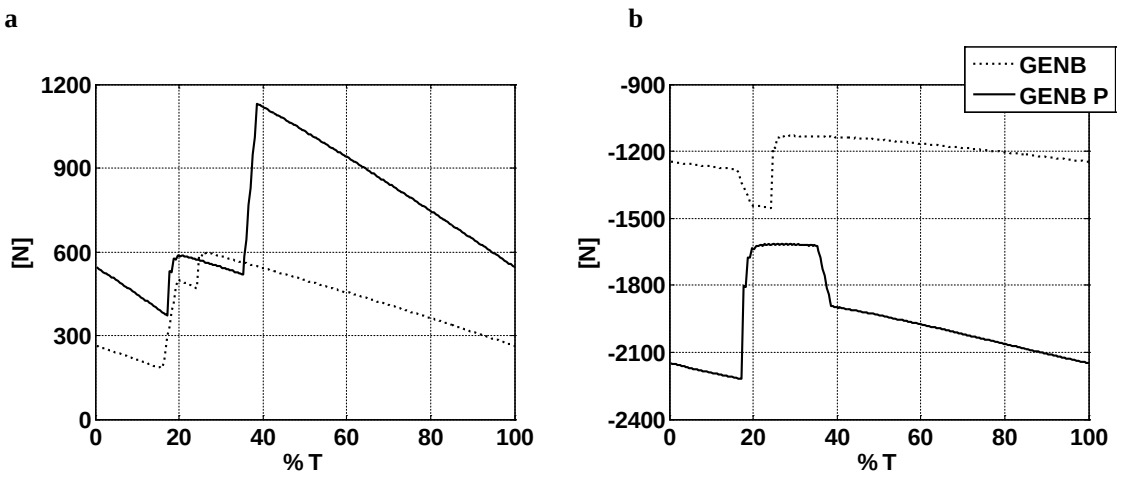

Figure 16. Pressure forces on gear 1 along (a) X_1 and (b) Y_1 directions at operational condition of 2000 rpm and 90 bar, for *GENB* and *GENB_P* pumps.

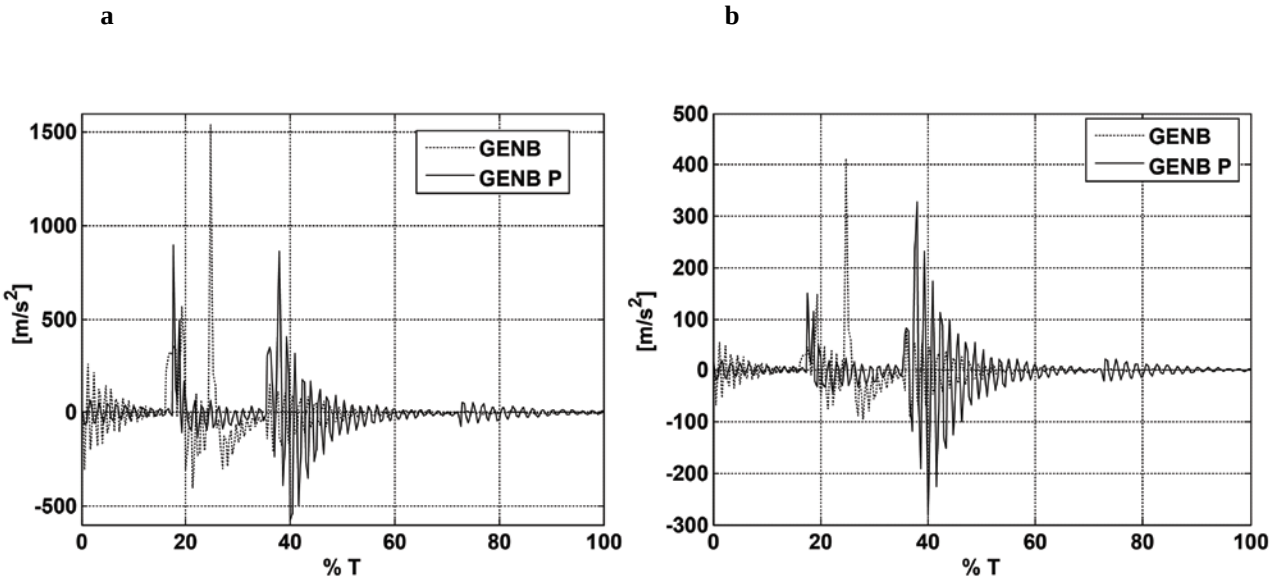

Figure 17. Accelerations on gear 1 in (a) X_1 and (b) Y_1 directions at operational condition of 2000rpm and 90 bar, for *GENB* and *GENB_P* pumps.

Table 1. Main model parameters for *GENB* and *GENB_P* gear pumps.

	Pump *GENB*	**Pump *GENB_P***
Number of teeth	z=12	z=11
Gear module [mm]	m = 1.15	m = 1.7
Helix angle on the pitch circle [deg]	β=0	β=4
Face width [mm]	b=12.1	b=14.9
Pressure angle [deg]	α =20	α =22
Pressure angle in working conditions [deg]	α_w =27.727	α_w =24.142
Contact ratio	$\tilde{\varepsilon}$ =1.35	$\tilde{\varepsilon}$ =1.7
Angles defining the ending of the isolated tooth spaces for gear 1 [deg].	$\Phi_{A1,}$ =339.68	Φ_{A1} =334.82
Angles defining the beginning of the isolated tooth spaces for gear 1 [deg].	Φ_{B1} =200.32	Φ_{B1} =205.18

Table 2. Natural Frequencies of the linearized model at 34 bar.

	34 bar - 2000 rpm	**34 bar - 2600 rpm**	**34 bar - 3200 rpm**	**34 bar - 3350 rpm**
f_{n1}[Hz]	3717	3750	3783	3792
f_{n2}[Hz]	4130	4130	4130	4130
f_{n3}[Hz]	5013	5055	5098	5109

Table 3. Natural Frequencies of the linearized model at 90 bar.

	90 bar - 2000 rpm	**90 bar - 2600 rpm**	**90 bar - 3200 rpm**	**90 bar - 3350 rpm**
f_{n1}[Hz]	4130	4130	4130	4130
f_{n2}[Hz]	5944	5963	5982	5987
f_{n3}[Hz]	8026	8051	8076	8083